

Femtosecond X-ray absorption spectroscopy in warm dense matter

B. Mahieu,^{1,*} N. Jourdain,^{2,3,*} K. Ta Phuoc,¹ F. Dorchie,²
J.-P. Goddet,¹ A. Lifschitz,¹ P. Renaudin,³ and L. Lecherbourg³

¹LOA, ENSTA ParisTech - CNRS - Ecole Polytechnique,
Université Paris-Saclay, 828 Boulevard des Maréchaux, 91120 Palaiseau, France

²Université de Bordeaux, CNRS, CEA, CELIA (Centre Lasers Intenses et Applications), UMR 5107, 33400 Talence, France

³CEA-DAM-DIF, 91297 Arpaçon, France

Exploring and understanding ultrafast processes at the atomic level is a scientific challenge¹⁻³. Femtosecond X-ray Absorption Spectroscopy (XAS) is an essential experimental probing technic, as it can simultaneously reveal both electronic and atomic structures, and thus unravel their non-equilibrium dynamic interplay which is at the origin of most of the ultrafast mechanisms. However, despite considerable efforts, there is still no femtosecond X-ray source suitable for routine experiments. Here we show that betatron radiation from relativistic laser-plasma interaction⁴ combines ideal features for femtosecond XAS. It has been used to investigate the non-equilibrium transition of a copper sample brought at extreme conditions of temperature and pressure by a femtosecond laser pulse. We measured a rise time of the electron temperature below 100 fs. This first experiment demonstrates the great potential of the betatron source and paves the way to a new class of ultrafast experiments.

X-ray absorption spectroscopy techniques are essential tools for probing both electronic and atomic structural properties of matter. Including X-ray Absorption Near-Edge Structure (XANES) and Extended X-ray Absorption Fine Structure (EXAFS), they are exploited in a wide range of applications in coordination chemistry, gas-phase systems, materials science or for the study of complex biological samples⁵. XAS has been extensively developed at synchrotrons, taking advantage of the broadband photon spectrum lying in the keV region, where most of elements absorption edges are located. When one aims at studying the temporal response of a sample after ultrafast excitation, referring to the time-resolved XAS technique, the temporal resolution of the observed phenomena becomes limited by the duration of the synchrotron pulses, *i.e.* $\sim 10 - 100$ ps, or the temporal resolution of streak camera, *i.e.* few ps. That leaves veiled the very first moments where the out-of-equilibrium interplay between still frozen atoms and strongly modified electrons drives the ultrafast processes. To date, two main solutions were tested to circumvent this limitation: synchrotron slicing, where a few hundreds femtosecond

temporal slice of the pulse is extracted to probe the sample at the cost of a greatly reduced photon flux^{6,7}, and wavelength scanning on a X-ray free-electron laser that requires a very large number of shots⁸. Some dispersive measurements have been reported, but they are limited to a few eV bandwidth, and must circumvent the inherent shot-to-shot spectral fluctuations of such a source⁹. Both options rely on the use of expensive large scale research instruments providing limited access, and the very large number of shots needed to recover a single absorption spectrum severely limits the range of systems and regimes that can be studied (continuously renewed targets, *e.g.* in liquid jets, or reversible phase transitions).

Here we present the first demonstration of femtosecond-resolved XAS using a table-top X-ray source naturally combining broad spectrum and femtosecond duration with required features in terms of stability, photon flux and inherent pump-probe synchronization. Our scheme relies on the betatron radiation from laser-plasma acceleration. While this source was to date too unstable for carrying out any realistic XAS study, we recently demonstrated the production of stable betatron radiation¹⁰ making it now possible. Time-resolved XAS experiment has been performed to investigate at the atomic scale the ultrafast dynamics of a copper foil brought from solid to warm dense matter (WDM) by a femtosecond optical laser pulse. Such study has been selected as a paragon of a strongly excited system, leading to the full ablation of the heated sample after a single shot. The complete experimental setup is described in Fig. 1.

WDM is a subject of increased interest due to its importance for planetary physics^{11,12}, inertial confinement fusion research¹³ and material science¹⁴. WDM is laying between solid and plasma, with a density close to the solid one and a temperature of a few 10^4 K. It is characterized by a partial disorder but with strong atom correlation and electron degeneracy, which make it challenging to simulate and predict properties. When produced in the laboratory by femtosecond isochoric heating of a solid foil, the energy is suddenly deposited in the electrons and is homogenized along the thickness in a femtosecond time scale^{15,16}. That leads to strong out-of-equilibrium situations where the electron temperature can reach tens of thousands K while the lattice is still cold. The electron-ion thermal equilibration follows on a longer time scale (a few ps). The electron dynamics of WDM has been experimentally studied from XAS, but so

* These two authors contributed equally to this work.

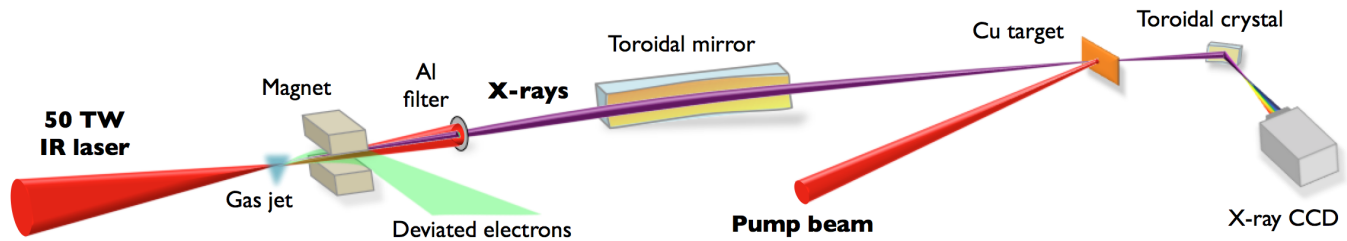


FIG. 1. *Setup of the experiment.* A 50 TW, 30 fs laser pulse is focused onto a supersonic jet of 99%helium / 1%nitrogen gas mixture. The interaction of the laser with the underdense created plasma yields the generation of a betatron X-ray pulse (see *Methods* for details). The latter is focused by a toroidal mirror on the Cu sample placed at normal incidence. A spectrometer composed of a toroidal crystal and an X-ray charge-coupled device (CCD) camera then records the transmitted spectrum. In parallel, a synchronized laser pulse (pump), with adjustable delay with respect to the X-ray pulse and with adjustable fluence, is used to heat the Cu sample up to the WDM regime. The absence of jitter is ensured by the fact that the pump laser and the laser-generated X-ray pulse originate from the same laser source.

far with only a few picosecond resolution, thus limiting the investigation to the long-lived relaxation dynamics of electron temperature¹⁷. The femtosecond dynamics of the electron heating and its homogenization, as well as the maximum temperature achieved, have remained unreachable until now.

Figure 2 presents results of numerical simulations of the system under study, corresponding to three successive snapshots: cold lattice before heating, strong out-of-equilibrium at the femtosecond time scale and electron-ion thermal equilibration in the picosecond regime. The copper L_3 and L_2 edges observed around 932 eV and 952 eV (Fig. 2d) respectively correspond to transitions from the $2p_{3/2}$ and $2p_{1/2}$ core levels up to unoccupied electron states in the continuum, just above the Fermi energy E_F . When the copper sample is heated by the pump pulse, electrons below E_F start to be excited up to higher energy levels, leaving some unoccupied states in the $3d$ band whose upper part is located $\sim 1-2$ eV below E_F . These unoccupied states allow new transitions from initial $2p$ to final $3d$ states, leading to additional absorption observed a few eV below the L-edges¹⁹ (Fig. 2e). This structure is called *pre-edge*.

Figure 3 presents XAS measurements obtained using the betatron source. Spectra corresponding to three selected pump-probe delays are shown, together with a “cold” absorption spectrum (without pump pulse). For negative delays, the probe pulse arrives before the pump pulse and the spectrum remains unchanged from the cold situation. For positive delays, an increasing absorption is observed below the cold absorption edges: this is the pre-edge structure predicted by the theory. The lower panel of Fig. 3 shows the difference between the measured absorption spectra of heated sample and the cold spectrum. It clearly emphasizes the presence of this rising pre-edge during the first hundreds fs that follow the pump laser irradiation.

It has been recently shown that one can measure the electron temperature T_e through this pre-edge²⁰. Taking advantage of careful numerical calculations, we have deduced the time evolution of T_e from the pre-edge spec-

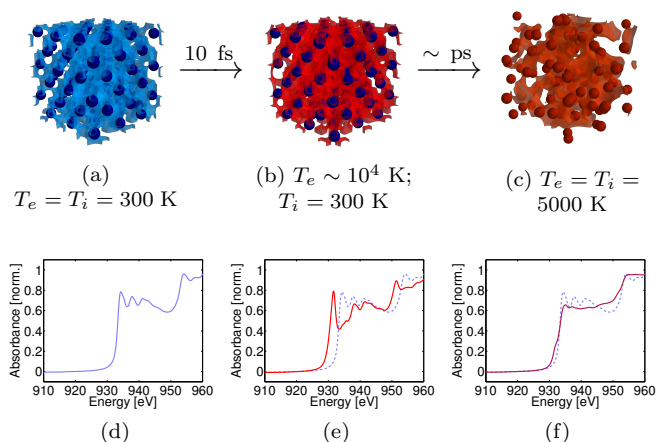


FIG. 2. *Ultrafast non-equilibrium transition from solid to WDM.* The energy of a femtosecond optical laser pulse is suddenly deposited in the electrons of the system (femtosecond scale), then progressively transferred to the lattice (picosecond scale). (a) Cold solid lattice before heating: the electron temperature T_e equals the ion one T_i . (b) Just after heating, a strongly out-of-equilibrium situation is transiently produced where electrons are hot while the lattice is still cold and solid-like. (c) A few picoseconds after, the lattice disappears as electrons and ions progress up to their thermal equilibration. (d)–(f) Calculated absorption spectra in the XANES region corresponding respectively to (a)–(c). The cold XANES signal shown in (d) is reported in dashed line in (e) and (f). Simulations made using the Abinit code¹⁸.

tral integration evaluated for each spectrum. Results are shown in Fig. 4. The electron temperature evolution is characterized by a fast femtosecond increase (corresponding to the sample heating) followed by a longer picosecond decrease (electron-ion thermal equilibration). Looking carefully at the first time steps, the rise-time is estimated at $\tau_{rise} = 75 \pm 25$ fs RMS, a little larger than the 30 fs expected from the heating pulse duration. On the same figure, we report the time evolutions

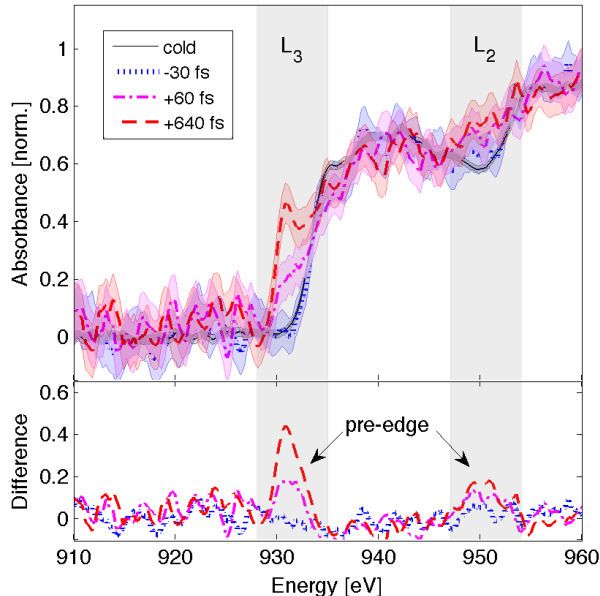


FIG. 3. *Time-resolved XAS data.* Selection of some measurements near the Cu L-edges (L_3 and L_2), without and with the pump pulse (incident fluence of 1 J/cm^2), for three different X-ray probe delays. *Upper panel:* Normalized X-ray absorbance. The shadowed area indicates the standard deviation of the measurements over a series of 50 consecutive shots. *Lower panel:* Differential absorbance with respect to the curve without pump. Clear pre-edges appear a few eV below the L-edges just after the sample heating.

of T_e and T_i calculated from a two-temperature hydrodynamic code (see *Methods*). The overall data are well reproduced by the model, including the maximal value of $T_e = 10000 \pm 2000 \text{ K}$. At the considered fluence, the calculation predicts that the melting occurs at $\sim 1 \text{ ps}$ after heating.

The overall temporal resolution of the measurement is the contribution of several parameters, among which the pump and probe durations – respectively measured at 30 fs and estimated at 9 fs FWHM (full-width at half maximum), see *Methods*. The pump beam forms a $\theta_x = 2.5^\circ$ angle with the X-ray beam and the measured horizontal X-ray beam size is $\sigma_x = 200 \pm 60 \mu\text{m}$ FWHM at the sample surface. This sets an additional geometrical contribution to the temporal resolution equal to $\sigma_x \cdot \theta_x / c = 30 \pm 10 \text{ fs}$, but not yet enough to reproduce the observation. One must thus consider the physical process of thermalization occurring within the sample in order to understand the nature of τ_{rise} . The energy deposition in the whole sample thickness can be divided in two steps²¹. Electrons are first excited in the near-surface region within the penetration depth ($\sim 15 \text{ nm}$ for copper at the wavelength of the pump laser); then, the energy is transported through the ballistic motion of electrons. Taking a characteristic electron velocity

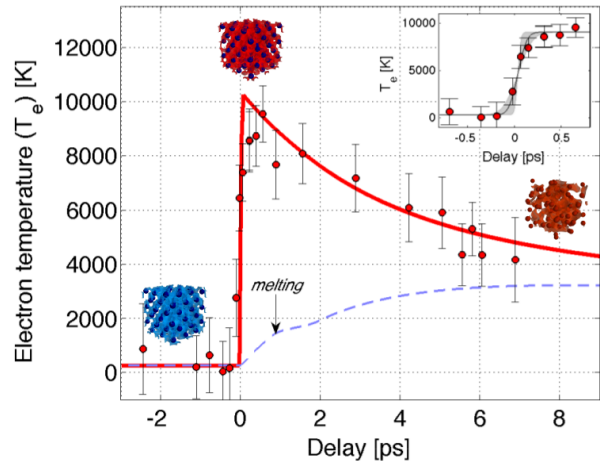


FIG. 4. *Time evolution of the electron temperature.* The data deduced from time-resolved XAS measurements (full circles) are compared with the two-temperature hydrodynamic calculation (plain line). The calculated ion temperature is also plotted (dashed line). The incident fluence is 1 J/cm^2 . The experimental data indicate a rise-time of $75 \pm 25 \text{ fs}$ (line and shadowed area in the inset). The gradual decrease observed at longer time is well reproduced by the model and is understood as the electron-ion thermal equilibration. Errorbars are calculated from the integrated standard deviation within the pre-edge in the XAS data series.

$v_e = v_F + \sqrt{k_B T_e / m_e}$, where k_B is the Boltzmann constant, m_e the electron mass and v_F the Fermi velocity, leads to $v_e \simeq 10^6 \text{ m/s}$. The critical parameter for the relevance of ballistic transport of the electrons is the electron mean free path d , which is governed by elastic, quasi-elastic and inelastic scattering. In copper $d = 70 \text{ nm}$ ²¹ and is approximately equal to the sample thickness so that homogeneous heating throughout the sample is ensured within a timescale comparable to the inelastic lifetime at optical excitation energies ($d/v_e \simeq 80 \pm 35 \text{ fs}$). Electron heating is thus the main contribution to our observation. Furthermore, the expected value of τ_{rise} given statistically by the quadratic sum of the different contributions listed hereabove (pump duration, probe duration, temporal limit given by the pump-probe angle, electron heating time) is equal to $90 \pm 40 \text{ fs}$, which is indeed in the range of our measurement.

In conclusion, we investigated the ultrafast and out-of-equilibrium transition of a copper foil brought from solid to warm dense matter by a femtosecond laser pulse. X-ray absorption spectra are registered near the L-edge with unprecedented femtosecond temporal resolution. For this, we rely on the production of stable betatron X-ray pulses from a laser-plasma accelerator, providing a few-femtosecond duration inferred from by the ionization-induced injection scheme. We measured a rise time of the electron temperature of $75 \pm 25 \text{ fs}$, larger than the estimated temporal resolution. It is under-

stood as the macroscopic energy diffusion time throughout the sample. Data are quite well reproduced by a two-temperature hydrodynamic calculation. It shows that the femtosecond resolution achieved allows to capture out-of-equilibrium situations before the melting, thus access to the intimate understanding of ultrafast phase transition physics. This first demonstration experiment opens new paths for studying matter under extreme conditions and ultrafast science in general²². In addition to its unique temporal resolution, betatron is a table-top synchrotron-like X-ray source which now offers new possibilities for a wide scientific community.

Methods

Laser beams The experiment was conducted at Laboratoire d’Optique Appliquée with the “Salle Jaune” Ti:Sapphire laser system, which delivers 2×1.5 J pulses at a central wavelength of 810 nm. One arm is used for betatron X-ray generation. It was focused into a 3 mm supersonic 99%He – 1%N₂ gas jet with a 1-m-focal-length off-axis parabola, to a focal spot size of ~ 15 μm (FWHM). A deformable mirror is used for improving the laser beam quality at focus. The second arm is used for sample heating. The laser presents a super-gaussian profile with 48 mm $1/e^2$ diameter. A 10-mm iris is placed 7 m before the sample, forming a top-hat intensity distribution. The iris plane is imaged onto the sample by means of a near-normal incidence 25-mm-focal-length spherical mirror placed 26.8 mm in front of the sample. This allows a transversely homogeneous heating of the sample over a $\pi \cdot 400$ μm^2 sample surface. The pump beam fluence on the sample was controlled by finely tuning the pump beam energy. The maximum pump fluence was 6.5 J/cm². The nominal laser pulse duration was measured to be 30 ± 5 fs (FWHM) by a spectral-phase interferometry for direct electric field reconstruction (SPIDER) apparatus. Grating spacing of the laser compressor stage was adjusted to obtain the same minimum pulse duration of the pump beam on the copper sample.

Betatron radiation The laser pulse focused in the gas jet creates an underdense plasma. Electrons from this plasma are accelerated in the wakefield of the laser, reaching energies of a hundred MeV. They follow an oscillating trajectory with typical transverse amplitude of 1 μm and longitudinal period of 150 μm . Due to this relativistic motion, they emit in the forward direction a low-divergence X-ray beam (~ 10 mrad) with a continuous spectrum extending up to about 10 keV. This is called the betatron radiation. We made use of the ionization injection scheme²³, ensuring the production of stable betatron radiation¹⁰. Typically, 10^5 photons/shot/0.1%BW are emitted around 1 keV²⁴.

X-ray pulse duration Since the accelerated electron bunch is confined just behind the laser pulse, the betatron source intrinsically provides ultrashort pulses. We calculated the temporal shape of the betatron X-ray

pulse using a particle-in-cell (PIC) simulation²⁵. For our parameter regime, accelerated electrons originate from the peak of the laser field only, where the L-shell of the nitrogen atoms are ionized. This localization ensures the production of a single electron bunch in the first wakefield cavity (see inset of Fig. 5). The PIC simulation gives a 6-fs long electron bunch (FWHM). We then calculated the X-ray temporal profile at 930 eV, corresponding to the energy of the copper L₃ absorption edge. The result is shown in Fig. 5, and gives a FWHM duration of 9 fs. This is slightly longer than the electron bunch duration, due to a slippage effect between the emitted photons travelling faster than the wiggling electrons. This effect is even emphasized for lower energy electrons, which need larger oscillations for emitting the same photon energy. These electrons, injected later in the accelerating cavity and thus positioned at the back end of the bunch, are responsible for the tail of the X-ray pulse profile that can be seen on Fig. 5.

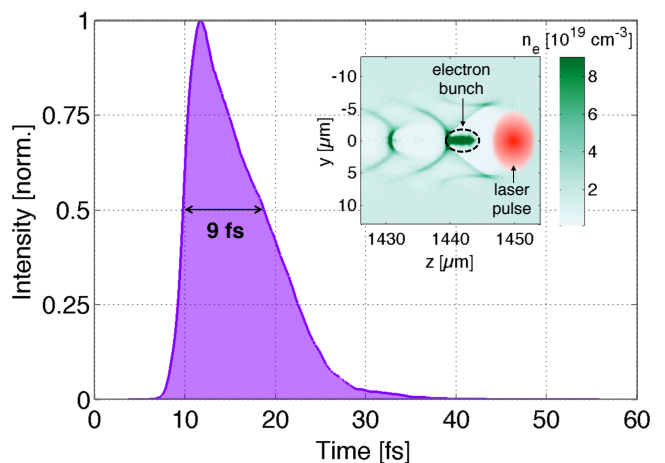


FIG. 5. *Result of particle-in-cell simulations.* Main curve: temporal X-ray profile calculated on-axis for 930-eV photons. Inset: Two-dimensional map of the plasma density n_e , showing the electron bunch accelerated in the wake of the laser pulse.

X-ray spectrometer A Bragg spectrometer was built for measuring the absorption spectra. It covers a 50 eV bandwidth centered around the L-edges of Cu (L₃ at 932 eV and L₂ at 952 eV). It consists of a toroidal RbAP crystal and a CCD camera placed at its sagittal focus, which coincides with the Rowland circle in order to have a spectral resolution independent of the X-ray source. A slit placed at the tangential focus of the crystal allows for noise removal due to the fluorescence of the crystal. The CCD is an in-vacuum water-cooled PI-MTE from Princeton Instruments ®. The crystal is curved with a sagittal radius of 85 mm, a tangential radius of 200 mm and was built by Saint-Gobain Crystals ®.

Sample and procedure A 70 ± 10 nm Cu layer was deposited on a 30×80 mm² area by evaporation on a 1- μm MylarTM foil strengthening the whole membrane.

Since the copper heated area is ablated after a single laser irradiation, the sample is moved to present a fresh surface shot after shot, allowing ~ 500 shots per membrane. An automatized procedure was implemented to trigger the laser shot, command the X-ray spectrometer acquisition and move the sample, with an effective repetition rate of 0.3 Hz. For sufficient data statistics and signal to noise ratio, 50 acquisitions were required per spectrum, completed by series of raw spectra (without sample) for normalization. After a pump-probe series, the ablated areas were scanned a second time by the x-rays in order to check the correct overlap between the pump and the probe beams.

XAS data extraction In order to recover each absorption spectrum, we registered 3 spectra (each one resulting from a series of 50 shots) : without sample (reference), with cold sample, and with heated sample. For each series, a median filter is applied in order to remove the residual hot spots noise. The 50 images are summed and the spectra are extracted from a line-out profile. The cold/heated transmissions are obtained from the division of the cold/pumped series over the reference one. The cold absorption spectrum (coming from the logarithm of the transmission) is then set to zero below the L_3 edge,

and normalized above the L_2 edge. The same normalization is used for the heated spectrum. The remaining error bars are mainly limited by the number of detected X-ray photons. Several spectra were measured under similar conditions (incident heating fluence and delay) in order to increase the statistics and reduce the error bars.

TTM simulations The two-temperature model (TTM) is used to calculate the evolution of the electron and ion temperatures T_e and T_i .²⁶ It is integrated in the one-dimensional hydrodynamic code ESTHER detailed in Ref.²⁷, that describes the matter evolution with multiphase equation of state²⁸ and consistent ion heat capacity. The electron heat capacity and electron-ion coupling parameter are taken from Lin et al.²⁹. A simplified approach is here considered for the laser energy absorption (homogeneous heating). The source term is a 30-fs FWHM Gaussian function with 0.15 J/cm^2 integrated fluence, that corresponds to 15% overall laser absorption calculated by solving the Helmholtz equations with an incident fluence of 1 J/cm^2 . The time required to homogenize the electron temperature along the sample thickness is not considered in this simulation. It is retrieved from the best fit of the experimental T_e rise-time τ_{rise} by a convolution of the TTM calculation with a Gaussian function.

-
- [1] Boutet, S. et al. High-resolution protein structure determination by serial femtosecond crystallography. *Science* **337**, 362–364 (2012).
- [2] Gerber, S. et al. Femtosecond electron-phonon lock-in by photoemission and x-ray free-electron laser. *Science* **357**, 71–75 (2017).
- [3] Pertot, Y. et al. Time-resolved x-ray absorption spectroscopy with a water window high-harmonic source. *Science* **355**, 264–267 (2017).
- [4] Rousse, A. et al. Production of a keV X-ray beam from synchrotron radiation in relativistic laser-plasma interaction. *Phys. Rev. Lett.* **93**, 135005 (2004).
- [5] Koningsberger, D. C. and Prins, R. *X-ray absorption: principles, applications, techniques of EXAFS, SEXAFS and XANES* J. Wiley & Sons, New York (1988).
- [6] Cavalleri, A. et al. Band-Selective Measurements of Electron Dynamics in VO_2 Using Femtosecond Near-Edge X-Ray Absorption. *Phys. Rev. Lett.* **95**, 067405 (2005).
- [7] Bressler, Ch et al. Femtosecond XANES study of the light-induced spin crossover dynamics in an iron (II) complex. *Science* **323**, 489–492 (2009).
- [8] Lemke, H. T. et al. Femtosecond X-ray absorption spectroscopy at a hard X-ray free electron laser: application to spin crossover dynamics. *J. Phys. Chem. A* **117**, 735–740 (2013).
- [9] Gaudin, J. et al. Towards simultaneous measurements of electronic and structural properties in ultrafast x-ray free electron laser absorption spectroscopy experiments. *Sci. Rep.* **4**, 4724 (2014).
- [10] Doepp, A. et al. Stable femtosecond X-rays with tunable polarization from a laser-driven accelerator *Light Sci. Appl.* **6**, e17086 (2017).
- [11] Guillot, T. Interiors of giant planets inside and outside the solar system. *Science* **286**, 72–77 (1999).
- [12] Wilson, H. F. and Militzer, B. Rocky core solubility in Jupiter and giant exoplanets. *Phys. Rev. Lett.* **108**, 111101 (2012).
- [13] Colin-Lalu, P. et al. Dissociation along the principal Hugoniot of the Laser Mégajoule ablator material. *Phys. Rev. E* **94**, 023204 (2016).
- [14] Ernstorfer, R. et al. The formation of warm dense matter: experimental evidence for electronic bond hardening in gold. *Science* **323**, 1033–1037 (2009).
- [15] Ogitsu, T. et al. Ballistic electron transport in non-equilibrium warm dense gold. *High Energ. Dens. Phys.* **8**, 303–306 (2012).
- [16] Widmann, K. et al. Single-State Measurement of Electrical Conductivity of Warm Dense Gold. *Phys. Rev. Lett.* **92**, 125002 (2004).
- [17] Cho, B. I. et al. Electronic Structure of Warm Dense Copper Studied by Ultrafast X-Ray Absorption Spectroscopy. *Phys. Rev. Lett.* **106**, 167601 (2011).
- [18] Gonze, X. et al. First-principles computation of material properties: the ABINIT software project. *Comput. Mater. Sci.* **25**, 478–492 (2002).
- [19] Dorchie, F. and Recoules, V. Non-equilibrium solid-to-plasma transition dynamics using XANES diagnostic. *Phys. Rep.* **657**, 1 (2016).
- [20] Cho, B. I. et al. Measurement of electron-ion relaxation in warm dense copper. *Sci. Rep.* **6**, 18843 (2016).
- [21] Hohlfeld, J. et al. Electron and lattice dynamics following optical excitation of metals. *Chem. Phys.* **251**, 237 (2000).

- [22] Albert, F. and Thomas, A. G. R. Applications of laser wakefield accelerator-based light sources. *Plasma Phys. Control. Fusion* **58**, 103001 (2016).
- [23] Pak, A. et al. Injection and trapping of tunnel-ionized electrons into laser-produced wakes. *Phys. Rev. Lett.* **104**, 025003 (2010).
- [24] Corde, S. et al. Femtosecond x rays from laser-plasma accelerators. *Rev. Mod. Phys.* **85**, 1 (2013).
- [25] Lifschitz, A. et al. Particle-in-Cell modelling of laser-plasma interaction using Fourier decomposition. *J. Comput. Phys.* **228**, 1803 (2009).
- [26] Anisimov, S. I., Kapeliovich, B. L. & Perelman, T. L. Electron Emission from Metal Surfaces Exposed to Ultrashort Laser Pulses. *Eksp. Teor. Fiz.* **66**, 375–377 (1974).
- [27] Colombier, J. P., Combis, P., Bonneau, F., Le Harzic, R. & Audouard, E. Hydrodynamic simulations of metal ablation by femtosecond laser irradiation. *Phys. Rev. B* **71**, 165406 (2005).
- [28] Bushman, A. V., Fortov, V. E. & Lomonosov, I. V. Models of wide-range equations of state for matter under conditions of high energy density, *Sov. Tech. Rev. B Therm. Phys.* **5**, 1 (1993).
- [29] Zhibin, L., Zhigilei, L. V. & Celli, V. Electron-Phonon Coupling and Electron Heat Capacity of Metals under Conditions of Strong Electron-Phonon Nonequilibrium. *Phys. Rev. B* **77**, 075133 (2008).

Acknowledgements

We thank Martine Millerieux for sample preparation and Vanina Recoules for support with the Abinit code. This work was funded by the Agence Nationale pour la Recherche through the FEMTOMAT Project No. ANR-13-BS04-0002 and the European Research Council through the X-Five grant (Contract No. 339128).